EARTH SURFACE PROCESSES AND LANDFORMS
Earth Surf. Process. Landforms **46**, 296–306 (2021)

Published online 16 November 2020 in Wiley Online Library
(wileyonlinelibrary.com) DOI: 10.1002/esp.5024

Impact of an 0.2 km³ Rock Avalanche on Lake Eibsee (Bavarian Alps, Germany) – Part I: Reconstruction of the paleolake and Effects of the Impact

Sibylle Knapp,[1]* Philipp Mamot,[1] Bernhard Lempe[2] and Michael Krautblatter[1]
[1] Landslides Research Group, Technical University of Munich, Munich, Germany
[2] Engineering Geology, Technical University of Munich, Munich, Germany

Received 25 March 2020; Revised 1 October 2020; Accepted 3 October 2020

*Correspondence to: Sibylle Knapp, Landslides Research Group, Technical University of Munich, Munich, Germany. E-mail: sibylle.knapp@tum.de

ESPL
Earth Surface Processes and Landforms

ABSTRACT: Rock avalanches destroy and reshape landscapes in only a few minutes and are among the most hazardous processes on Earth. The surface morphology of rock avalanche deposits and the interaction with the underlying material are crucial for runout properties and reach. Water within the travel path is displaced, producing large impact waves and reducing friction, leading to long runouts. We hypothesize that the 0.2 km^3 Holocene Eibsee rock avalanche from Mount Zugspitze in the Bavarian Alps overran and destroyed Paleolake Eibsee and left a unique sedimentological legacy of processes active during the landslide. We captured 9.5 km of electrical resistivity tomography (ERT) profiles across the rock avalanche deposits, with up to 120 m penetration depth and more than 34 000 datum points. The ERT profiles reveal up to ~50 m thick landslide debris, locally covering up to ~30 m of rock debris with entrained fine-grained sediments on top of isolated remnants of decametre-wide paleolake sediments. The ERT profiles allow us to infer processes involved in the interaction of the rock avalanche with bedrock, lake sediments, and morainal sediments, including shearing, bulging, and bulldozing. Complementary data from drilling, a gravel pit exposure, laboratory tests, and geomorphic features were used for ERT calibration. Sediments overrun by the rock avalanche show water-escape structures. Based on all of these datasets, we reconstructed both position and size of the paleolake prior to the catastrophic event. Our reconstruction of the event contributes to process an understanding of the rock avalanche and future modelling and hazard assessment. Here we show how integrated geomorphic, geophysical, and sedimentological approaches can provide detailed insights into the impact of a rock avalanche on a lake. © 2020 The Authors. Earth Surface Processes and Landforms published by John Wiley & Sons Ltd

KEYWORDS: rock avalanche; runout; lake impact; paleolake reconstruction; ERT calibration; water-escape structures; Northern Calcareous Alps; Eibsee; Zugspitze

Introduction

Massive rock-slope failures cause more than 60% of all catastrophic landslide disasters (Evans et al., 2006). The interaction of the rockslide and rock avalanche material with the substrate over which they travel strongly influences runout properties (e.g. Abele, 1994; Hungr and Evans, 2004; Dufresne et al., 2010; Robinson et al., 2015). Erodible and deformable substrates as well as obstacles may divide the rock avalanche into multiple lobes, and their deposits often show complex emplacement structures with longitudinal and transverse ridges (Hewitt, 2006; Dufresne et al., 2015; Dufresne et al., 2016). Water reduces basal friction of the sliding mass, resulting in increased runout velocity and length (Abele, 1997; Erismann and Abele, 2001; Legros, 2006). Large landslides that enter lakes or other water bodies have generated disastrous waves up to several 100 m high (e.g. Lituya Bay; Fritz et al., 2009). Landslide-triggered waves may also transform into debris avalanches or debris flows that endanger human lives and infrastructure over a wide area (Iverson et al., 1997; Walter et al., 2020). Researchers have analysed landslide-triggered impact waves in the laboratory (e.g. Evers and Hager, 2016; Miller et al., 2017), reconstructed displacement waves by numerical modelling (e.g. Kafle et al., 2016; Gylfadóttir et al., 2017), and provided insights into the sedimentology of impact-wave deposits (e.g. Roberts et al., 2013; Dufresne et al., 2018).

In spite of the scientific progress described earlier, the reconstruction and modelling of ancient events often remain challenging, and become speculative, as researchers are confronted with a lack of data on paleotopography, substrate characteristics, and the possible involvement of water. If the landslide mass is large relative to water depth, much of the water in a lake will be pushed out of the impact zone rather

than entrained (e.g. Miller et al., 2017). In such cases, the resulting landform may resemble that of dry rock avalanches, even though they ran out on water-saturated sediments or entered a lake (Shaller, 1991). Water-escape structures within sediments overrun by landslides may provide evidence of water (Pavoni, 1968; Lowe, 1975; Yarnold, 1993), but the basal contact between the rock avalanche deposits and underlying substrates are rarely accessible (Dufresne et al., 2015). Hence, geomorphic evidence is often used to infer the presence and role of water in massive rock-slope failures (Plafker and Ericksen, 1978; Shaller, 1991; Siebert, 2002). This approach, however, can be problematic for high-energy events because the water may not become fully incorporated into the streaming debris.

To date, no study has documented sedimentology that reveals the spatial and temporal reconstruction of a rock avalanche that has entered a lake and displaced its water. In this article, we focus on this issue by presenting evidence for the existence and size of a paleolake in the German Alps that was overrun by a rock avalanche. We marry geomorphological mapping with a geoelectrical survey and sedimentological analysis of outcrops and drillhole data to prove the existence of this paleolake and to provide an estimation of its size. The geoelectrical profiles provide insights into the structure,

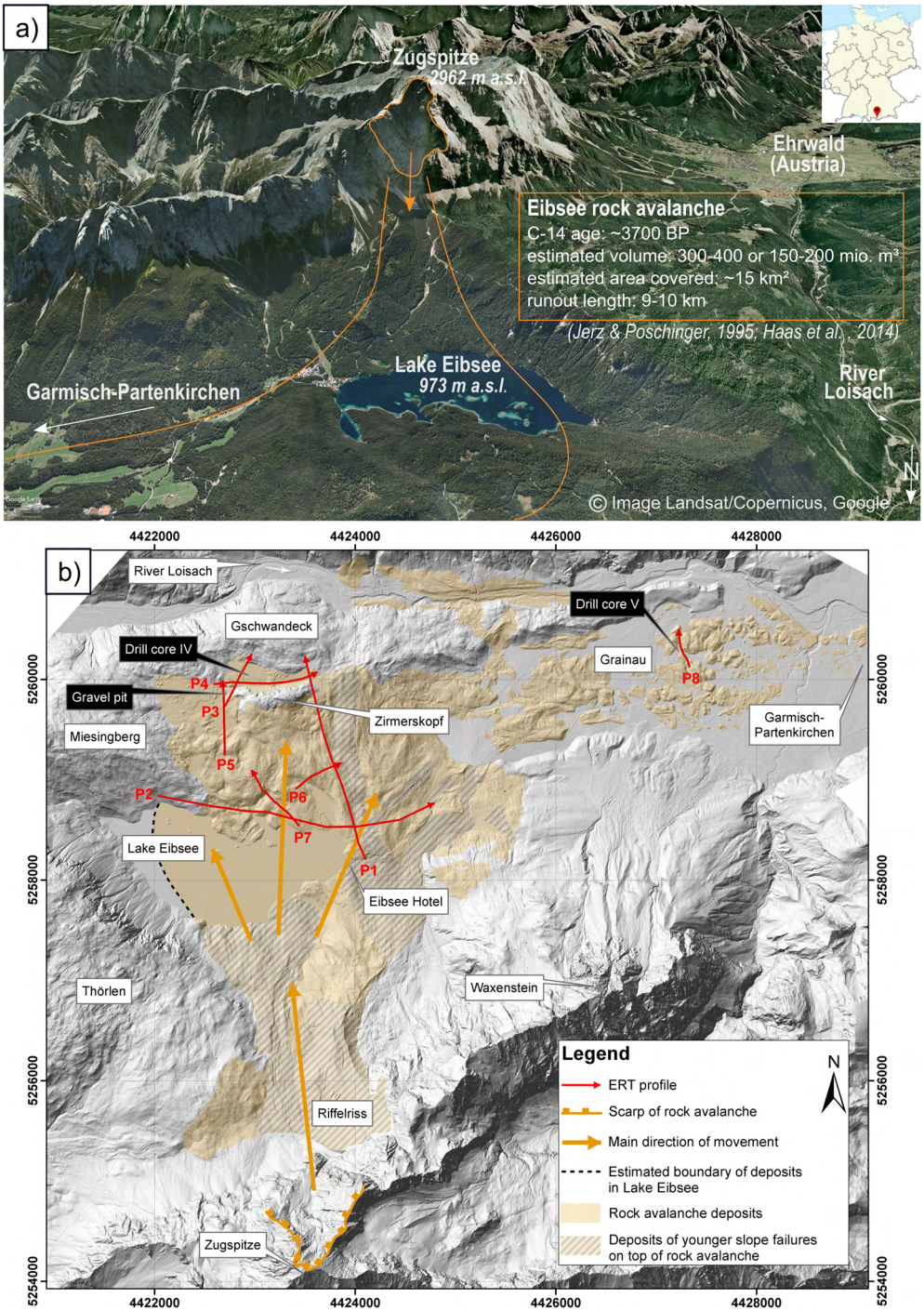

Figure 1. (a) Satellite image with a three-dimensionalview of the Wetterstein Mountains in southern Germany, showing Mount Zugspitze (2962 m a.s.l.) and the scarp of the Eibsee rock avalanche, modern Lake Eibsee and part of the runout zone towards Garmisch-Partenkirchen. (b) LiDAR image (hillshade) with overview of the scarp niche Bayerisches Schneekar at Mount Zugspitze and the area covered with rock-slope failure deposits. The locations of ERT profiles P1–P8 are shown as red lines. Coordinates are given in Gauss-Krüger Zone 4 (Bavarian Surveying and Mapping Authority, 2006). [Colour figure can be viewed at wileyonlinelibrary.com]

thickness, and distribution of the rock avalanche deposits and their interaction with lake water and lake sediments. Our results offer an explanation for the exceptionally long runout of the rock avalanche (9–10 km; Jerz and Poschinger, 1995) and support our paleotopographic reconstruction, thus providing a valuable contribution to future modelling and hazard assessment.

Lake Eibsee and Mount Zugspitze

Geographical setting and geology

Lake Eibsee is located in the Wetterstein Mountains in the southernmost part of Bavaria at an elevation of 973 m above sea level (a.s.l.). It lies at the foot of Mount Zugspitze, the highest summit in Germany at 2962 m a.s.l. (Figure 1a). This area is of considerable research interest as it lies at the edge of the Northern Calcareous Alps and is prone to large rock-slope failures in carbonate rocks (Krautblatter et al., 2012). The rock avalanche that is the subject of this article detached from the scarp niche 'Bayerisches Schneekar' on the north flank of Mount Zugspitze. The Zugspitze comprises Triassic limestones and dolostones of the dislocated and overthrust Wamberg Anticline (Rüffer, 1995; Haas et al., 2014). The Eibsee Syncline, over which these rocks have been thrust, are Jurassic and Cretaceous limestones and dolostones with low permeability that favour the presence of a paleolake on the valley floor (Tollmann, 1976; Hornung and Haas, 2017).

Eibsee rock avalanche

The Eibsee rock avalanche is the largest rock-slope failure in Bavaria (Abele, 1974). The landslide deposit covers an area of ~15 km^2 and has a runout length of 9-10 km and a maximum vertical travel distance of ~2.3 km (Jerz and Poschinger, 1995; Haas et al., 2014).

Volume estimates range from 400-600 million m^3 (Abele, 1974; Prager et al., 2008) and 300–400 million m^3 (Jerz and Poschinger, 1995) to 150–200 million m^3 (Haas et al., 2014; Leith et al., 2016). Vidal (1953) initially interpreted the debris to be glacial, but Abele (1974) recognized them to be rock avalanche deposits. The main flow direction is to the north, but a large lobe extends to the east towards Garmisch-Partenkirchen (Figure 1). Jerz and Poschinger (1995) obtained a radiocarbon age that dates the event to ~3700 BP (Part II, the companion to this article, Knapp et al., 2020). They inferred that the landslide had overridden a lake based on the presence of displaced lake clay in a drillcore, and accordingly suggested that the long runout resulted from the involvement of the lake waters. Haas et al. (2014) proposed a paleolake situated at the same location as modern Lake Eibsee. However, the displaced clay site is far from the modern lake, and the existence and size of a paleolake remained speculative.

Methods

Geomorphological mapping

Geomorphological mapping was performed at a scale of 1:10 000 on airborne laser-scan images and topographic maps. A bare-earth digital elevation model (DEM) with 1-m resolution was provided by the Bavarian Surveying and Mapping Authority (2006). We mapped characteristic landforms of the rock avalanche deposits, distinguishing between longitudinal and transverse ridges and valleys. To evaluate landslide flow directions, we covered the study area with a grid of 200-m--wide cells. The 200-m cells divided ridges and valleys into smaller segments. A ridge or valley was classified as 'longitudinal' if it diverges no more than 30° from the mean flow direction of the segment, and 'transverse' if it diverges no more than 30° from the orthogonal to that direction. An 'undefined' orientation refers if the angle relative to the mean flow direction is 30°–60°.

Electrical resistivity tomography (ERT)

We performed an electrical resistivity tomography (ERT) survey with an ABEM SAS 1000 Terrameter with 81 electrodes. The roll-along method was employed along eight two-dimensional profiles (Figure 1b, Supporting Information Table S1) with electrode spacings of 5 m and 4 m using 100-m-long cables, as well as one profile with a 10 m electrode spacing using 200-m-long cables. All measurements were made with Wenner and Schlumberger arrays and the same current settings (up to 200 mA and 400 V, respectively). The contact resistance of each electrode was tested before measurements were started.

Data were processed with the inversion software RES2DInv (Loke, 2006) in three steps: (i) bad datum points (few outliers) were eliminated; (ii) the data were inverted using robust inversion to avoid smoothing the resistivity gradients (Sass, 2004); and (iii) in the case of profile P8, we used a finer mesh size to cope with high-resistivity contrasts (Krautblatter and Hauck, 2007) and inverted the data with a half electrode spacing of 2.5 m.

The ERT profiles were calibrated in the field where data from drillings and outcrops are available, and the measured values of apparent resistivity were cross-checked with laboratory data on the different rock types (Plattenkalk Limestone, Wetterstein Limestone and Hauptdolomite).

Sedimentological analysis

A detailed sedimentological analysis was undertaken in a gravel pit northwest of Mount Zirmerskopf to facilitate the recognition and characterization of distal rock avalanche deposits. Two sediment samples of matrix-rich bands were analysed by wet sieving using the Euronorm DIN EN ISO 17892-4 (2017-04) protocol and classified based on their fractal dimension (Xu et al., 2001; Dufresne and Dunning, 2017). The results are presented using DCSIEVE software.

Results and Interpretation

The results of the complex flow behaviour of the Eibsee rock avalanche can be seen in deposit morphology, bulk material composition related to mixing or entrainment of substrate material and water (ERT), and rock avalanche lithofacies (sedimentology).

Rock avalanche landforms and interpretation

Geomorphic mapping revealed several features characteristic of rock avalanches (Figure 2). Parallel or radiating ridges with small valleys or depressions in between can be found throughout the study area. The longitudinal ridges, oriented towards the north, are common. The ridge surfaces are covered with limestone mega-blocks that derived from the scarp niche

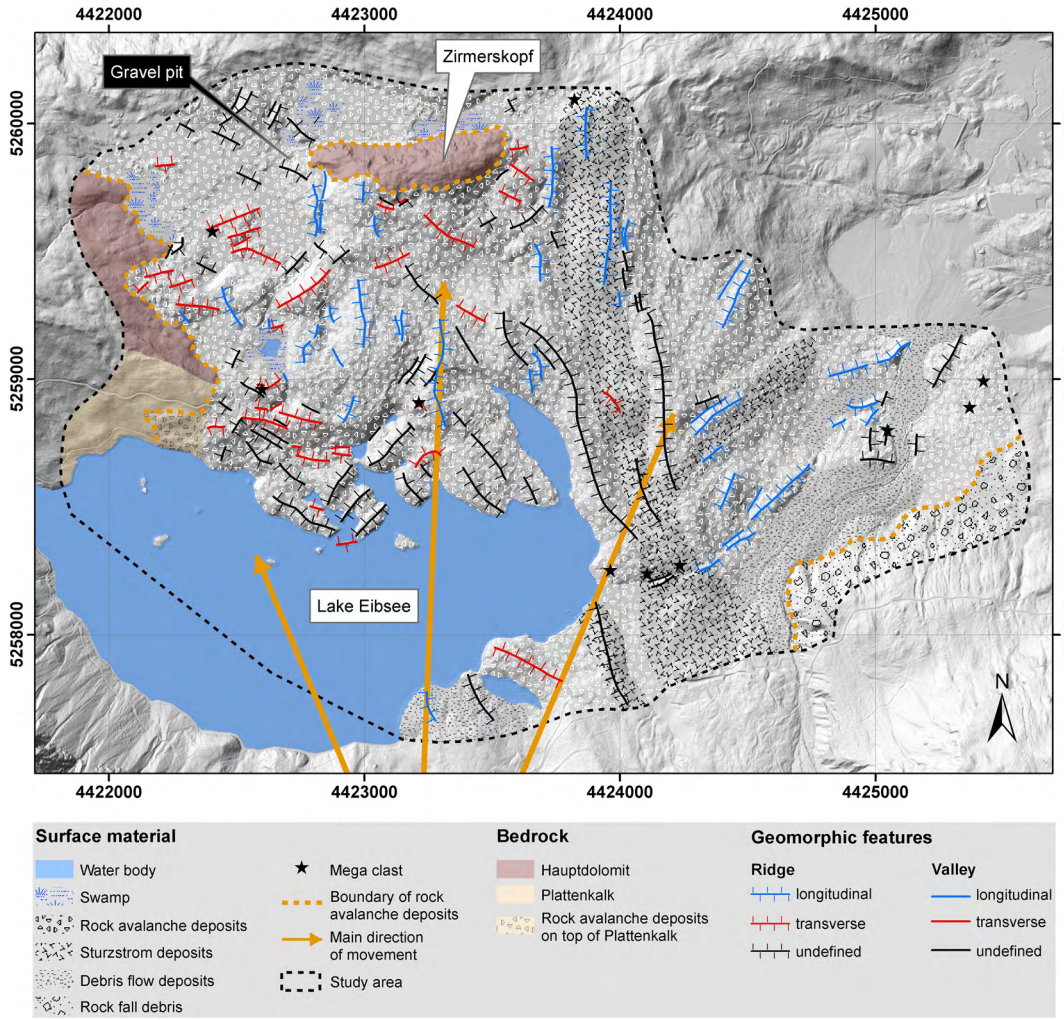

Figure 2. Geomorphic map of rock avalanche, rock fall, and debris flow deposits, showing the main direction of movement and longitudinal and transverse ridges and valleys. LiDAR image: Bavarian Surveying and Mapping Authority (2006); coordinates given in Gauss-Krüger Zone 4. [Colour figure can be viewed at wileyonlinelibrary.com]

(Wetterstein Limestone), many of them exceeding 10 m in diameter. The largest blocks, with diameters of 20 m, lie along the main flow path. All ridges consist entirely of rock avalanche debris. Debris flows and sturzstrom-like debris flow deposits are present locally on top of the rock avalanche deposits (Hornung and Haas, 2017). Swamps are present at the west margin of the rock avalanche adjacent to bedrock slopes and north of Mount Zirmerskopf.

Topographic interference leads to longitudinal and transverse confinement of a rock avalanche (Hewitt, 2006; Dufresne et al., 2015). Longitudinal and transverse ridges can be interpreted to be pressure ridges (Hewitt, 2006) and record the deflection of debris by valley walls and obstacles as defined by Heim (1932) and related 'caroming' flow (Hewitt, 2006). The western half of the deposit has a chaotic orientation of ridges, indicating a complex interaction with topography, whereas ridges in the eastern half are mostly longitudinal and are parallel to the flow direction, probably because there were few obstacles along their path. The sturzstrom-like debris flow ran straight to the north without spreading, thus forming longitudinal ridges only.

Geophysical insights into the pre-failure landscape and the rock avalanche impact on a paleolake

Eight ERT profiles (location in Figure 1b) totalling ~9.5 km in length and with 34 000 resistivity datum points provide unprecedented insights into the rock avalanche deposits and the surface on which the deposits lie.

The profiles, shown in Figures 3 and 4, are depicted with the same colour ramp for ease of comparison. Minimum and maximum plots (MinMax-Plots) of all profiles are included in the Supporting Information (Figures S1 and S2) to show the uncertainties in the ERT measurements. Resistivity calibrations based on data from the literature, field, and laboratory tests are given in Table S2.

Four resistivity zones can be distinguished in Figures 3 and 4:

1 High resistivity zones (> 2000 Ωm, dark red): bedrock, either limestone (Plattenkalk or Wetterstein Formation) or dolomite (Hauptdolomite Formation). The rock avalanche carapace is highly resistive because of the large size and proximity of boulders.
2 Mid-range resistivity zone (~500–2000 Ωm, orange-red): mixed fine- and coarse-grained materials with a high proportion of boulders; interpreted to be moraine material covering bedrock. Mid-range resistivity is also encountered at the transition between high and low resistivity zones.
3 Low resistivity zone (~100–500 Ωm, yellow-blue): mixed fine- and coarse-grained materials with a high proportion of fines; interpreted to be highly fragmented rock avalanche debris mixed with entrained fine-grained (paleolake) sediments.
4 Extremely low resistivity zone (< 100 Ωm, dark blue): clay- or silt-size sediment, perhaps, mixed with small amounts of sand and small gravel; interpreted to be paleolake sediments.

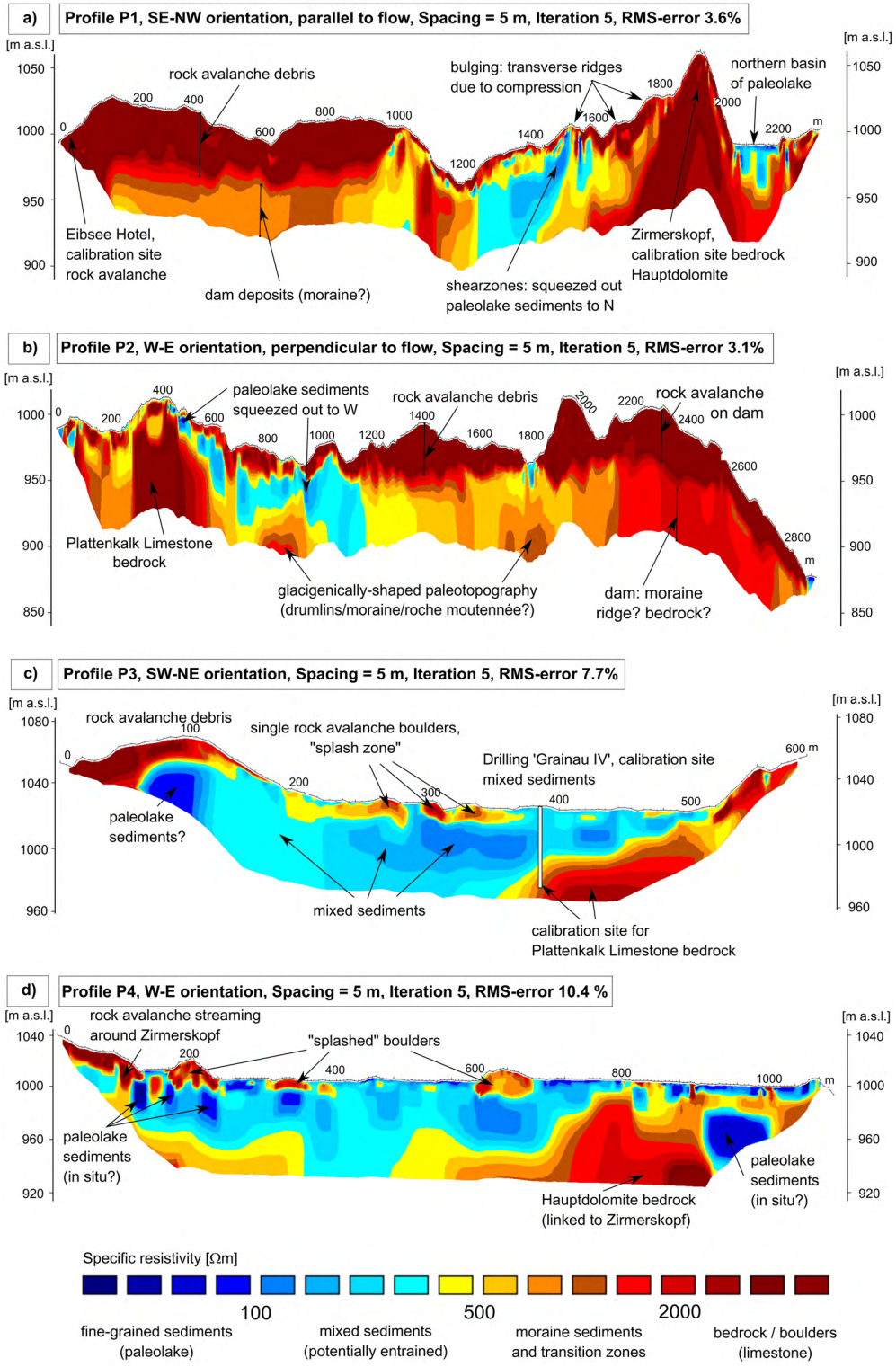

Figure 3. ERT profiles P1–P4. (a) P1: southeast–northwest (SE–NW) profile (in flow direction) of main deposits and bedrock at Mount Zirmerskopf. (b) P2: west–east (W–E) profile (perpendicular to flow direction) of main deposit between bedrock (W) and dam (E), showing shearing and squeezing out of paleolake sediments. (c) and (d) P3 and P4 showing the northern basin with 'splash zone', water-saturated mixed sediments and assumed*in situ*paleolake clays. [Colour figure can be viewed at wileyonlinelibrary.com]

Eight types of materials and processes detected with ERT could be calibrated in the field (Table S2): (i) rock avalanche body, (ii) bedrock (pk and hd), (iii) lake clay/silt and (iv) mixed sediments as materials, as well as processes like (v) bulldozing with (vi) overriding of secondary lobes, (vii) bulging, and (viii) splashing of single boulders. For these, calibration sites have been introduced in Figures 3 and 4. Moreover, morainal sediments, and upward injection of lake sediments are identified.

P1 (Figure 3a) is a profile oriented from south to north, in the direction of the incoming rock avalanche. At the south end of the profile, the surficial layer with mega-blocks can be calibrated at the Eibsee Hotel (Table S2; Socco et al., 2010). Here, the rock avalanche deposits are ~50 m thick and lie on top of material with mid-range resistivity (brown-red colour). We interpret the latter material to be morainal deposits (Table S2; Samouëlian et al., 2005) and/or bedrock that impound a

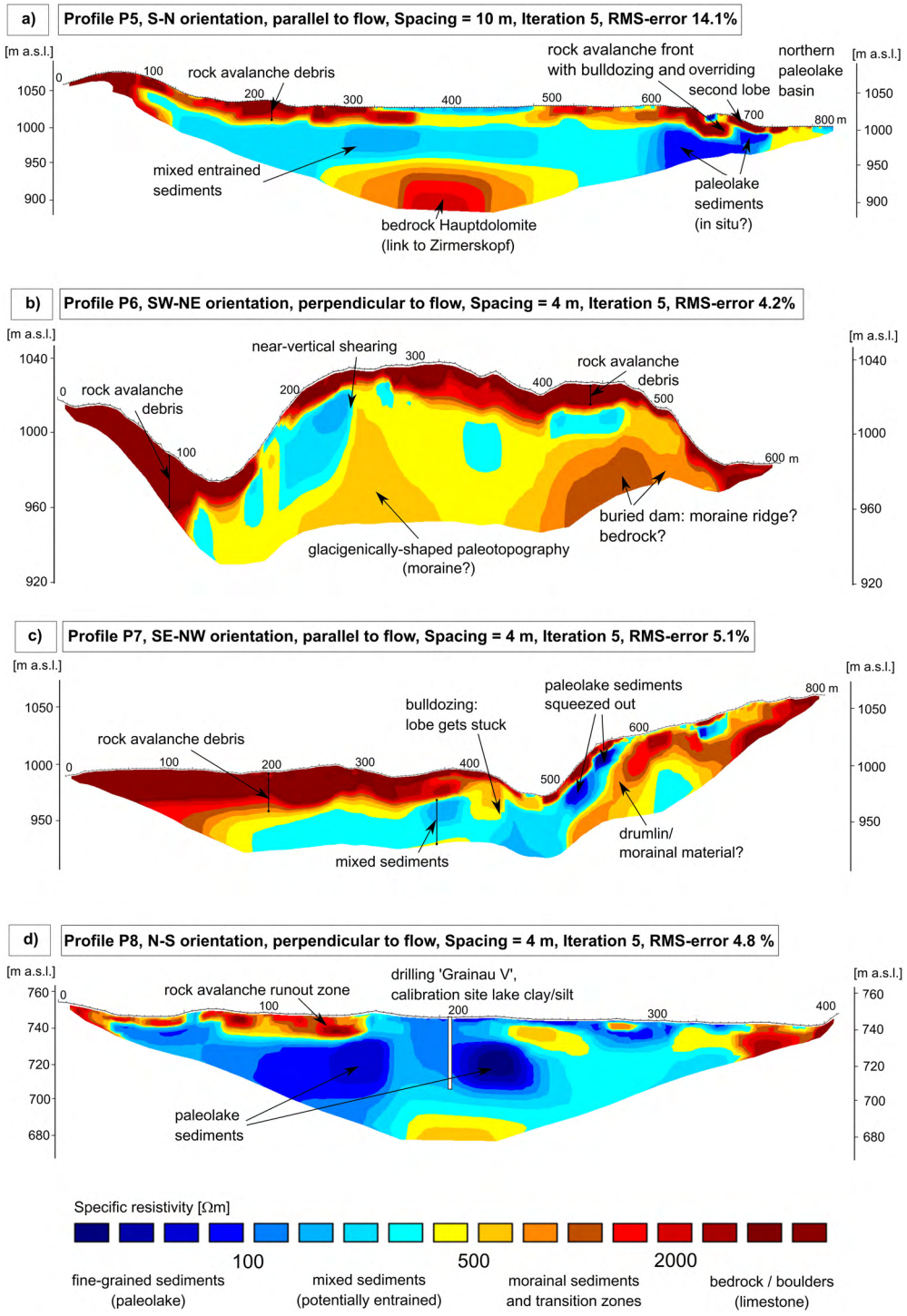

Figure 4. ERT-profiles P5–P8. (a) P5: ~120 m deep paleolake basin. (b) and (c) P6 and P7: details of shearing processes and paleotopography. (d) P8: the calibration site for lake clays with extremely low resisitivity values (< 100 Ωm, dark blue). [Colour figure can be viewed at wileyonlinelibrary.com]

paleolake towards the east. In the middle part of the profile are near-vertical shear zones with material of very low resistivity (< 100 Ωm, dark blue colour). This material is interpreted to be lake sediment squeezed into and partially mixed with rock avalanche [~100–400 Ωm, light blue colour; interpretation follows Bader (1979, 1981), Kneisel (2003) and Samouëlian et al. (2005)].

There is shearing due to compression (pressure ridges in Figure 2) during collision of the rock avalanche with bedrock at Mount Zirmerskopf (dark red colour). The ~30 m deep northern basin of the paleolake is seen at the north end of the profile with a thin cover of rock avalanche debris.

P2 (Figure 3b) extends in an easterly direction across the northern basin. The profile starts on the west on Plattenkalk Limestone bedrock (Table S2). Farther east, fine-grained material (~100 Ωm, blue colour) has been carried to the surface along shear zones, as is seen in P1. In the middle of the profile, rock avalanche debris overlies mixed sediments (~500 Ωm, yellow colour). The brown-red spots near the base of the profile in this area may delineate paleotopography shaped by glaciers (drumlins or flutings). At the east end, the profile extends across the paleodam observed in P1 (red colour), beyond which the surface elevation drops rapidly.

P3 (Figure 3c) and P4 (Figure 3d) provide views of the northern part of the paleolake. P3 passes the drilling site 'Grainau IV' (Jerz and Poschinger, 1995), where rock avalanche material is mixed with paleolake sediments and where the resistivity of Plattenkalk Limestone was calibrated. Large boulders at the

surface are sparse and not connected to the main rock avalanche deposit farther south. In P4, large boulders are stacked atop one another and extend upward without any indication of flowing motion. This area may rather be a 'splash zone' (e.g. Plafker and Ericksen, 1978; Cruden and Hungr, 1986) where boulders overtopped Mount Zirmerskopf at high speed and came to rest in the northern paleolake basin while rock avalanche material streamed around the ridge on both its west and east sides [homogenous debris; interpretation follows Ostermann et al. (2012)]. The stacked boulders overlie dark blue (< 100 Ωm) *in situ* paleolake sediments.

P5 (Figure 4a) is another northerly oriented profile parallel to flow that ends at the distal margin of the rock avalanche, with evidence of bulldozing at the front. In the middle part of the profile, we identify Hauptdolomite bedrock at ~100–120 m depth, suggesting that the basin was ~100 m deep at this locality after deglaciation.

P6 (Figure 4b) provides insight into the structure of the paleodam and translational shearing resulting from collision of the rock avalanche with the dam. Two near-vertical obstacles (red colour), which may be moraine material, are covered by ~20–30 m of rock avalanche debris with entrained fine-grained sediments (~100–500 Ωm, blue-yellow colour).

P7 (Figure 4c) is a short northwest-profile through ~30-m-thick rock avalanche deposits. One debris lobe has been overridden by a second lobe. Paleolake sediments (< 100 Ωm, dark blue) have been injected upward as the debris ran up a former hill (moraine ridge or drumlin).

P8 (Figure 4d) is located near the east end of the rock avalanche deposit at the 'Grainau V' drillsite (Jerz and Poschinger, 1995), where we calibrated ERT measurements in lake sediments (< 100 Ωm, dark blue). Thin rock avalanche deposits are registered in red.

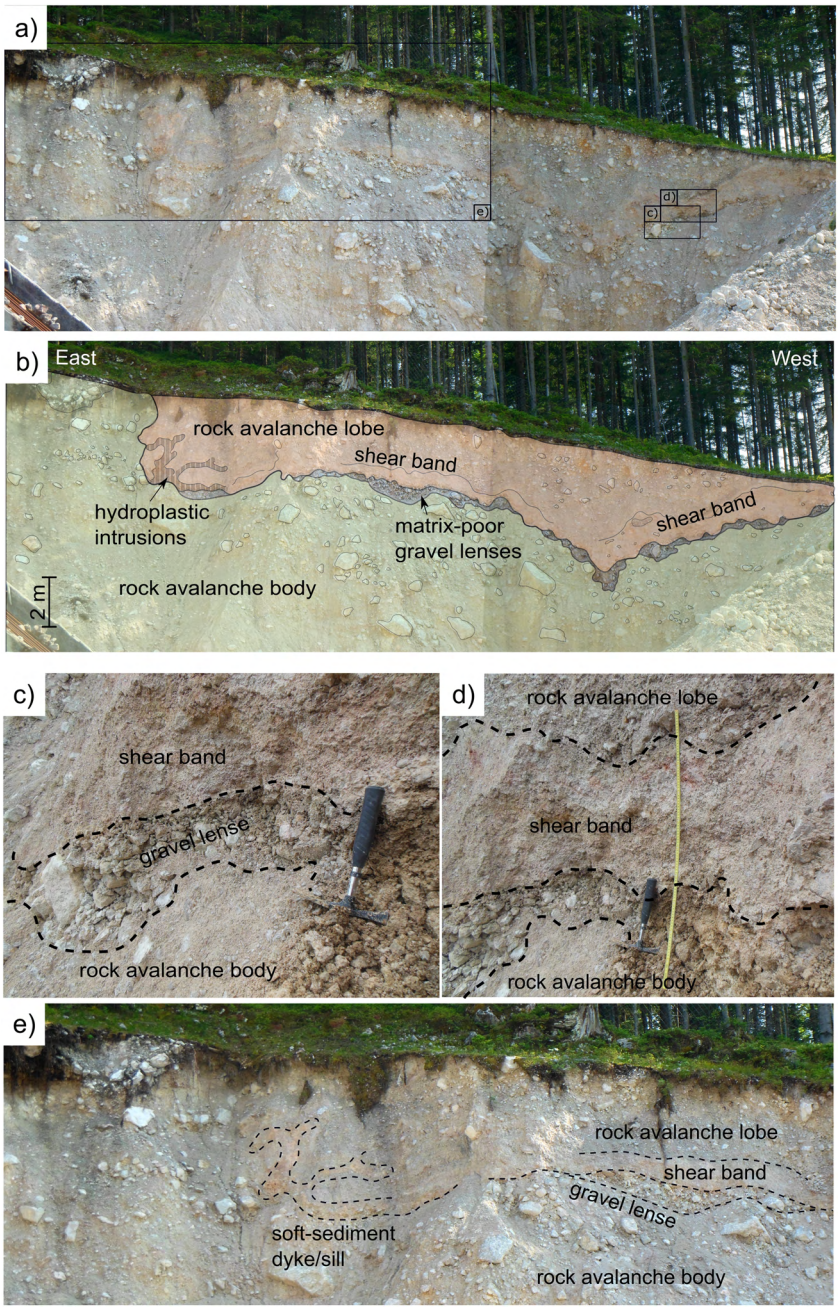

Figure 5. Gravel pit exposure at Mount Zirmerskopf. (a) and (b) Two lobes of rock avalanche debris separated by (c) and (d) reddish shear bands and gravel lenses. (e) Convoluted structures in the shear band. (Original photographs are provided in Figure S3 in the Supporting Information.) [Colour figure can be viewed at wileyonlinelibrary.com]

Shear zones and water-escape structures revealed in sediments

A gravel pit is located in a distal facies of the rock avalanche deposit west of Mount Zirmerskopf (Figure 1). The gravel pit provides a panoramic view ~30 m wide and ~10 m high of a blocky carapace and main body of the rock avalanche deposit with a paleoflow direction towards the observer (Figure 5). The base of the deposit is not visible. In the eastern half of the outcrop, the body of the rock avalanche deposit is covered by large boulders of Wetterstein Limestone. To the west, however, there are two sheets of diamictic rock avalanche deposits separated by a matrix-rich band, but without a distinct carapace (Figure 5a, b). Both sheets of rock avalanche debris have the same composition, but the lower sheet contains larger boulders than the upper one. The smaller fragments are angular to subangular and intensely fractured. The matrix-rich band is at the surface at the west end of the exposure, dips eastward down to ~3–4 m depth, then rises again and reaches the surface in the middle of the exposure (Figure 5a, b; for original photographs see Figure S3 in the Supporting Information).

The matrix-rich band consists of matrix-supported gravel, and is up to ~1.0 m thick (Figure 6). It has a reddish-orange tint that differentiates it from the light grey diamictic rock avalanche deposits. Contorted sill- and dyke-like structures are evident at the eastern termination of the band (Figure 5e). Here, the matrix-rich band shows complicated folding and penetration of the overlying rock avalanche material in multiple flame, diapir and injection structures. Matrix-free and matrix-poor gravel lenses locally sharply separate the matrix-rich band from the underlying rock avalanche deposits (Figure 5). The lenses are only few decimetres thick, are structureless, and contain stones that are more rounded than those in the body facies (Figure 5c, d).

The two rock avalanche bodies are interpreted to be the deposits of two, nearly simultaneous lobes. This interpretation is supported by ERT profile P5 (Figure 4a), where the outcrop is depicted at ~650 m length with up to ~30 m of rock avalanche deposits that have been bulldozed at the front of the rock avalanche. A thin front lobe overlies and presumably overran an initial thicker lobe. This happened when the first lobe slowed down while bulldozing as it entered the northern basin of the paleolake. The matrix band is interpreted to be a zone of shearing between these two lobes. Two sieved samples from the shear band (Figures 6 and S4) have fractal dimension factors of ~2.59 and ~2.72, typical of shear bands according to Dufresne and Dunning (2017). The fine-grained matrix is likely a product of comminution during fragmentation (Yarnold, 1993; Davies and Mcsaveney, 2009), but it might also contain entrained fines.

The convoluted sill- and dyke-like structures at the east edge of the shear band are interpreted to be soft-sediment deformation structures that formed due to water escape (Hewitt, 2006) and can be considered hydroplastic intrusions (Lowe, 1975). We attribute the convolution to shear-induced liquefaction as the flow decelerates (Bennett et al., 2000; Carling, 2013). The gravel lenses are likely wedges of debris bulldozed and washed out close to the front of the upper rock avalanche lobe as it ran out, when great hydraulic pressures were generated in the trapped moisture (Krieger, 1977; Yarnold, 1993). They can only form when water under high pressure entrains and removes fines, not by pore-water escape from wet substrates.

Discussion

ERT error sources

For the ERT survey, we used Wenner and Schlumberger arrays, which provides the best compromise between measurement precision and time investment (Rödder and Kneisel, 2012). The electrode arrangement provides high resistivity resolution in the vertical direction, but there is uncertainty in precision in the horizontal direction (Aizebeokhai, 2010). Additional uncertainties relate to (i) bad connections between the electrodes and substrate material, (ii) dryness of the sediment or (iii) large air-filled cavities, for example around rock avalanche boulders in the carapace (Supper et al., 2014). With regard to the first cause of uncertainty, it is important to push the nails thoroughly into the ground and remove loose sediment or plant cover prior to making measurement. We obtained sharp resistivity contrasts between rock avalanche material (~500–2000 Ωm, red),

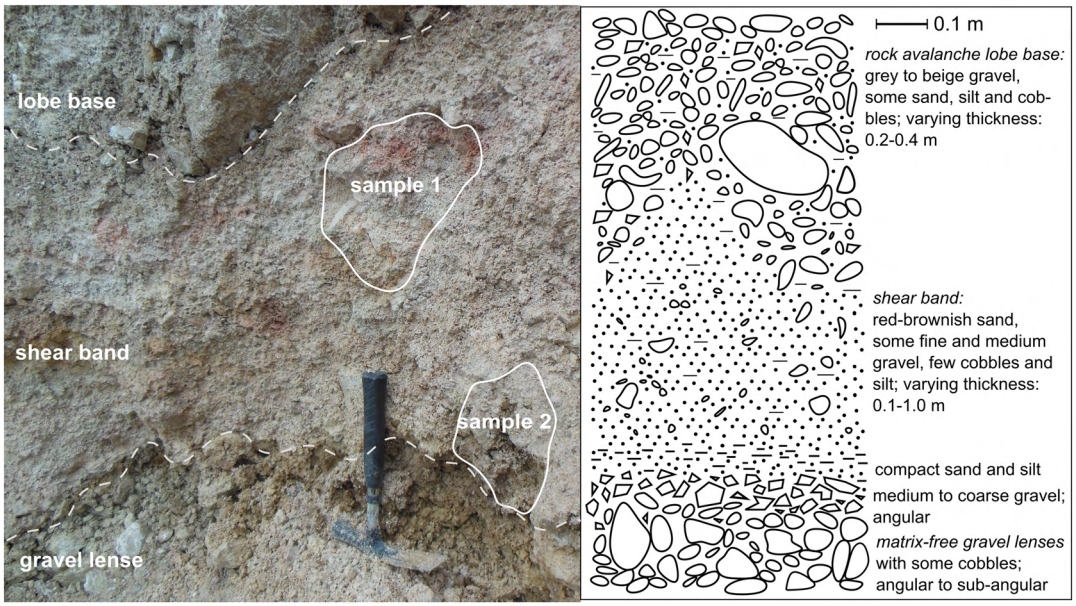

Figure 6. Sampling locations within shear band between two rock avalanche lobes. Sieving results are provided in Figure S4 in the Supporting Information. [Colour figure can be viewed at wileyonlinelibrary.com]

fine-grained lake sediments (< 100 Ωm, dark blue) and the mixed sediments (~100–500 Ωm, blue-yellow) in between.

The deviation between the measured values and the final tomography is indicated by the root mean square (RMS) error. Small errors do not necessarily indicate a realistic model (Hauck and Mühll, 2003), therefore we selected only five iterations of modelling rather than risking overfitting, while obtaining satisfying RMS errors between 3.1% and 14.1%. To further assess the reliability of the inversions, we created MinMax-Plots of the ERT uncertainty (Figures S1 and S2) based on a model covariance matrix (Alumbaugh and Newman, 2000). These plots show negligible uncertainty with respect to the interpreted sections.

Evidence that the rock avalanche impacted a lake

Complex emplacement structures with longitudinal and transverse ridges point toward the Eibsee rock avalanche impacting a deformable substrate (interpretation follows Hewitt, 2006; Dufresne et al., 2010; Dufresne et al., 2015). Swamps on the west and north margins of the rock avalanche deposit indicate water-impermeable geological strata, which favour the existence of a lake at this position.

Extremely low resistivity values below the rock avalanche deposit in the ERT profiles are indicative of lake sediments, which we calibrated with similar sediments encountered in drilling at 'Grainau V' (Jerz and Poschinger, 1995) and with data from the literature (Table S2). Moreover, zones of mixed deposits are present in distal areas where the rock avalanche moved into an existing lake. This is also supported by water-escape structures in the gravel pit at Mount Zirmerskopf (Figure 5). The matrix-free gravel lenses below the matrix-rich zone in this exposure indicate that the lake was filled with water and not dry (Yarnold, 1993).

Paleolake Eibsee

During the Last Glacial Maximum, the study area was covered by the Inn glacier flowing from the crest of the Alps (Fernpass area). When the glacier retreated, it left behind a landscape shaped by glacial erosion and partly blanketed by till and meltwater deposits. Till and/or bedrock formed a dam that sealed off part of the Eibsee Syncline (P1, P2 and P6; Figures 3 and 4). A lake formed behind the dam, and fine-grained lake sediments began to accumulate in it. The lake formed adjacent to the roche moutonnée Zirmerskopf (Figure 7a) near where late-glacial lake sediments, mobilized and redeposited by the rock avalanche, were found during the drilling at 'Grainau IV' (Jerz and Poschinger, 1995). To the west, the lake presumably reached the rising slope of Plattenkalk Limestone bedrock. At the south, the modern Lake Eibsee basin was also part of the paleolake, again dammed to the west and south by Plattenkalk Limestone. The paleolake existed and continued to accumulate silt and clay up to the moment of the Eibsee rock avalanche (Figure 7b; see Part II, the companion to this article, Knapp et al., 2020).

Interaction of the rock avalanche with the lake

Upon impact with the valley floor, the rock avalanche split into several lobes radiating fanwise across the valley floor. The centre of the rock avalanche impacted the paleolake and probably generated a displacement wave that moved north, east, and west.

The streaming rock mass eroded the floor of the lake but then slid on the fine-grained lake sediments. The basal friction was reduced due to lubrication or partial fluidization, probably causing the rock avalanche to accelerate. The eastern part of the rock avalanche decelerated as it crossed the rough and hilly terrain of the paleolake dam, and continued down the valley towards Garmisch-Partenkirchen. Lake sediments were entrained and mixed into the coarser, diamictic rock avalanche material (yellow and blue mid-range ERT values, Figures 3 and 4).

Due to collision with obstacles the rock avalanche split into several smaller lobes along its distal margins (Figures 4a, c, and 5). Bulldozing, squeezing, and shearing are recorded in the deposits at the margins of the paleolake. Here, multiple shear planes developed as successive lobes ran into one another with little time between them (P1 and P2; Figure 3). Also, soft-sediment deformation structures and water-escape

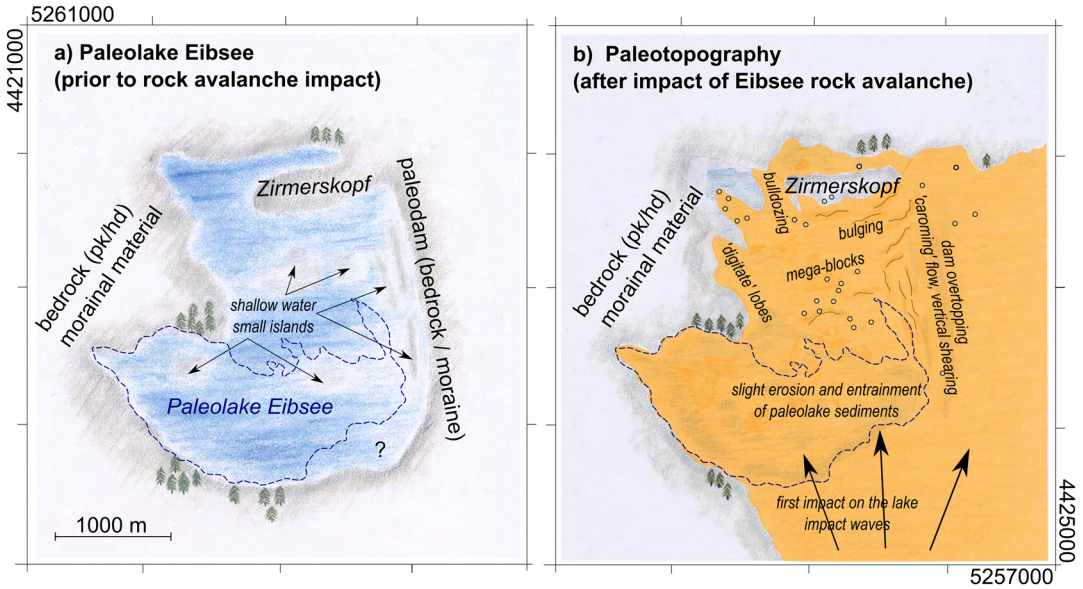

Figure 7. (a) Schematic sketch of Paleolake Eibsee with assumed dimension and position of the paleodam and shallow water areas and small islands. (b) Paleotopography after the rock avalanche impacts the lake, showing inferred processes. Dashed line indicates outline of modern Lake Eibsee. Coordinates are given in Gauss-Krüger Zone 4. [Colour figure can be viewed at wileyonlinelibrary.com]

structures formed where the rock avalanche ran over water-saturated fine-grained sediment.

Conclusions

The Eibsee rock avalanche overran Paleolake Eibsee. The entire body of water in the lake was displaced by the rock avalanche, presumably causing a large impact wave.

Fine-grained paleolake sediments were eroded and entrained by the rock avalanche. Water-escape structures, soft-sediment deformation structures, and matrix-free gravel lenses provide additional evidence for the existence of Paleolake Eibsee.

The paleolake was larger than modern Lake Eibsee. The main deposits of the rock avalanche cover the northern half of the paleolake. Today, swamps along the north and northwest sides of Lake Eibsee hint at the existence of the paleolake.

The long runout of the rock avalanche is attributed to low basal friction induced by entrainment of water and fine-grained sediments.

The rock avalanche deposits show evidence of complex runout and emplacement processes. Geomorphic mapping and an ERT survey provide detailed insights into interactive processes of the rock avalanche and the lake: separation into lobes, bulldozing, and formation of multiple shear planes at the lake margins with upward injection of fine-grained lake sediments.

We reconstructed the paleotopography of the valley before the rock avalanche. Resistivity values typical of morainal sediments were measured at the paleodam and along ridges and hilly landforms in the former basin of the proglacial paleolake.

Acknowledgements—Sibylle Knapp acknowledges PhD funding awarded by the German National Academic Foundation (Studienstiftung des deutschen Volkes e.V.). The authors thank Andreas von Poschinger for providing detailed information on the drillhole logs, and Ulrich Haas for discussions drawing from his lengthy experience in the Werdenfels region, particularly around Lake Eibsee. The authors also thank Christoph Wichert, Tobias Kriesmair, Julia Gottfriedsen, and Mathias Schimpfle for their help with the ERT field survey and laboratory work in context of their diploma theses at the Technical University of Munich. Finally, the authors thank Simone Herrmann (forest ranger), Jonas Kiesel and Falk Lempe for their support with fieldwork. Open access funding enabled and organized by Projekt DEAL.

Competing Interests

The authors declare that they have no conflict of interest.

Data Availability Statement

The data sets used and/or analysed during the current study are available from the corresponding author on reasonable request.

References

Abele G. 1974. Bergstürze in den Alpen. Ihre Verbreitung, Morphologie und Folgeerscheinungen. *Wissenschaftliche Alpenvereinshefte* **25**: 1–230.

Abele G. 1994. Large rockslides: their causes and movement on internal sliding planes. *Mountain Research and Development* **14**: 315–320.

Abele G. 1997. Rockslide movement supported by the mobilization of groundwater-saturated valley floor sediments. *Zeitschrift fuer Geomorphologie* **41**(1): 1–20.

Aizebeokhai AP. 2010. 2D and 3D geoelectrical resistivity imaging: Theory and field design. *Scientific Research and Essays* **5**(23): 3592–3605.

Alumbaugh DL, Newman GA. 2000. Image appraisal for 2-D and 3-D electromagnetic inversion. *Geophysics* **65**(5): 1455–1467.

Bader K. 1979. Exarationstiefen würmeiszeitlicher und älterer Gletscher in Südbayern (Trennung eisvorbelasteter und nicht eisvorbelasteter Sedimente aufgrund der seismischen Geschwindigkeiten). *E&G – Quaternary Science Journal* **29**(1): 49–62.

Bader K. 1981. Die glazialen Übertiefungen im Saalachgletscher-Gebiet zwischen Inzell und Königssee. *E&G – Quaternary Science Journal* **31**(1): 37–52.

Bavarian Surveying and Mapping Authority. 2006. *Airborne laser scan (Garmisch)*. Bavarian Surveying and Mapping Authority: München.

Bennett MR, Huddart D, McCormick T. 2000. The glaciolacustrine landform–sediment assemblage at Heinabergsjökull, Iceland. *Geografiska Annaler. Series A, Physical Geography* **82**(1): 1–16.

Carling PA. 2013. Freshwater megaflood sedimentation: What can we learn about generic processes? *Earth-Science Reviews* **125**: 87–113.

Cruden D, Hungr O. 1986. The debris of the Frank Slide and theories of rockslide–avalanche mobility. *Canadian Journal of Earth Sciences* **23** (3): 425–432.

Davies T, McSaveney M. 2009. The role of rock fragmentation in the motion of large landslides. *Engineering Geology* **109**(1-2): 67–79.

DIN EN ISO 17892-4. 2017-04. Geotechnical investigation and testing – Laboratory testing of soil – Part 4: Determination of particle size distribution (ISO 17892-4:2016); German version EN ISO 17892-4:2016.

Dufresne A, Dunning S. 2017. Process dependence of grain size distributions in rock avalanche deposits. *Landslides* **14**(5): 1555–1563.

Dufresne A, Davies T, McSaveney M. 2010. Influence of runout-path material on emplacement of the Round Top rock avalanche, New Zealand. *Earth Surface Processes and Landforms: The Journal of the British Geomorphological Research Group* **35**(2): 190–201.

Dufresne A, Prager C, Clague JJ. 2015. Complex interactions of rock avalanche emplacement with fluvial sediments: field structures at the Tschirgant deposit, Austria. In *Engineering Geology for Society and Territory*, Vol. **2**. Springer: Berlin; 1707–1711.

Dufresne A, Prager C, Bösmeier A. 2016. Insights into rock avalanche emplacement processes from detailed morpho-lithological studies of the Tschirgant deposit (Tyrol, Austria). *Earth Surface Processes and Landforms* **41**(5): 587–602.

Dufresne A, Geertsema M, Shugar D, Koppes M, Higman B, Haeussler P, Stark C, Venditti JG, Bonno D, Larsen C, Gulick SPS, McCall N, Walton M, Loso MG, Willis MJ. 2018. Sedimentology and geomorphology of a large tsunamigenic landslide, Taan Fiord, Alaska. *Sedimentary Geology* **364**: 302–318.

Erismann TH, Abele G. 2001. *Dynamics of rockslides and rockfalls*. Springer Science & Business Media: Berlin.

Evans SG, Mugnozza GS, Strom A, Hermanns RL, Ischuk A, Vinnichenko S. 2006. Landslides from massive rock slope failure and associated phenomena. In *Landslides from massive rock slope failure*. Springer: Berlin; 3–52.

Evers FM, Hager WH. 2016. Spatial impulse waves: Wave height decay experiments at laboratory scale. *Landslides* **13**(6): 1395–1403.

Fritz HM, Mohammed F, Yoo J. 2009. Lituya Bay landslide impact generated mega-tsunami 50th Anniversary. In *Tsunami Science Four Years after the 2004 Indian Ocean Tsunami*. Springer: Berlin; 153–175.

Gylfadóttir SS, Kim J, Helgason JK, Brynjólfsson S, Höskuldsson Á, Jóhannesson T, Harbitz CB, Løvholt F. 2017. The 2014 L ake A skja rockslide-induced tsunami: Optimization of numerical tsunami model using observed data. *Journal of Geophysical Research, Oceans* **122**(5): 4110–4122.

Haas U, Ostermann M, Sanders D, Hornung T. 2014. Quaternary sediments in the Werdenfels region (Bavaria, southern Germany). In *From the Foreland to the Central Alps – Excursion Guide to the Field Trips of the DEUQUA Congress in Innsbruck, Austria, 24-29 September 2014*, Kerschner H, Krainer K, Spötl C (eds). Geozon: Berlin; 18–30.

Hauck C, Mühll DV. 2003. Inversion and interpretation of two-dimensional geoelectrical measurements for detecting permafrost in mountainous regions. *Permafrost and Periglacial Processes* **14**(4): 305–318.

Heim A. 1932. *Bergsturz und menschenleben*. Fretz & Wasmuth: Zurich.

Hewitt K. 2006. Rock avalanches with complex run out and emplacement, Karakoram Himalaya, Inner Asia. In *Landslides from massive rock slope failure*. Springer: Berlin; 521–550.

Hornung T, Haas U. 2017. *Erläuterungen zur Geologischen Karte 1:25 000, 8531/8631 Zugspitze 8532/8632 Garmisch-Partenkirchen*. Bavarian Environmental Agency: Augsburg.

Hungr O, Evans S. 2004. Entrainment of debris in rock avalanches: an analysis of a long run-out mechanism. *Geological Society of America Bulletin* **116**(9-10): 1240–1252.

Iverson RM, Reid ME, LaHusen RG. 1997. Debris-flow mobilization from landslides. *Annual Review of Earth and Planetary Sciences* **25** (1): 85–138.

Jerz H, Poschinger A v. 1995. Neuere Ergebnisse zum Bergsturz Eibsee-Grainau. *Geologica Bavarica* **99**: 383–398.

Kafle J, Pokhrel PR, Khattri KB, Kattel P, Tuladhar BM, Pudasaini SP. 2016. Landslide-generated tsunami and particle transport in mountain lakes and reservoirs. *Annals of Glaciology* **57**(71): 232–244.

Knapp S, Anselmetti FS, Lempe B Krautblatter M. (2020) Impact of an 0.2 km³ Rock Avalanche on Lake Eibsee (Bavarian Alps, Germany) – Part II: Catchment Response to Consecutive Debris Avalanche and Debris Flow. *Earth Surface Processes and Landforms*. https://doi.org/10.1002/esp.5025

Kneisel C. 2003. *Electrical resistivity tomography as a tool for geomorphological investigations-some case studies (with 7 figures and 1 table)*. Zeitschrift für Geomorphologie, Supplement 132; 37–49.

Krautblatter M, Hauck C. 2007. Electrical resistivity tomography monitoring of permafrost in solid rock walls. *Journal of Geophysical Research – Earth Surface* **112**(F2): 1–14.

Krautblatter M, Moser M, Schrott L, Wolf J, Morche D. 2012. Significance of rockfall magnitude and carbonate dissolution for rock slope erosion and geomorphic work on Alpine limestone cliffs (Reintal, German Alps). *Geomorphology* **167**: 21–34.

Krieger MLH. 1977. *Large landslides, composed of megabreccia, interbedded in Miocene basin deposits, southeastern Arizona*, Vol. **1008**. US Government Printing Office: Washington, DC.

Legros F. 2006. Landslide mobility and the role of water. Landslides from massive rock slope failure. Edited by SG Evans, G. Scarascia Mugnozza, A. Strom, and RL Hermanns. NATO Sciences Series, IV. *Earth and Environmental Science* **49**: 233–242.

Leith K, Hofmayer F, Kessler B, Krautblatter M. 2016. *Preconditioning of the Eibsee rock avalanche by deglaciation and development of critical bedrock stresses*. Paper presented at the EGU General Assembly Conference Abstracts.

Loke M. 2006. RES2DINV ver. 3.55, Rapid 2-D resistivity & IP inversion using the least-squares method. *Software Manual*, 1–139.

Lowe DR. 1975. Water escape structures in coarse-grained sediments. *Sedimentology* **22**(2): 157–204.

Miller GS, Andy Take W, Mulligan RP, McDougall S. 2017. Tsunamis generated by long and thin granular landslides in a large flume. *Journal of Geophysical Research, Oceans* **122**(1): 653–668.

Ostermann M, Sanders D, Ivy-Ochs S, Alfimov V, Rockenschaub M, Römer A. 2012. Early Holocene (8.6 ka) rock avalanche deposits, Obernberg valley (Eastern Alps): Landform interpretation and kinematics of rapid mass movement. *Geomorphology* **171**: 83–93.

Pavoni N. 1968) Über die Entstehung der Kiesmassen im Bergsturzgebiet von Bonaduz-Reichenau (Graubünden). *Ecl. Geologic. Helvetica* **61**(2): 494–500.

Plafker G, Ericksen G. 1978. Nevados Huascaran avalanches, Peru. In *Developments in Geotechnical Engineering*, Vol. **14**. Elsevier: Amsterdam; 277–314.

Prager C, Zangerl C, Patzelt G, Brandner R. 2008. Age distribution of fossil landslides in the Tyrol (Austria) and its surrounding areas. *Natural Hazards and Earth System Sciences* **8**: 377–407.

Roberts NJ, McKillop RJ, Lawrence MS, Psutka JF, Clague JJ, Brideau M-A, Ward BC. 2013. Impacts of the 2007 landslide-generated tsunami in Chehalis Lake, Canada. In *Landslide science and practice*. Springer: Berlin; 133–140.

Robinson TR, Davies TR, Reznichenko NV, De Pascale GP. 2015. The extremely long-runout Komansu rock avalanche in the Trans Alai range, Pamir Mountains, southern Kyrgyzstan. *Landslides* **12**(3): 523–535.

Rödder T, Kneisel C. 2012. Permafrost mapping using quasi-3D resistivity imaging, Murtèl, Swiss Alps. *Near Surface Geophysics* **10**(2): 117–127.

Rüffer T. 1995. *Entwicklung einer Karbonat-Plattform: Fazies, Kontrollfaktoren und Sequenzstratigraphie in der Mitteltrias der westlichen Nördlichen Kalkalpen (Tirol, Bayern)*. Heidelberg: Geologisch-Paläontologisches Institut der Ruprecht-Karls-Universität.

Samouëlian A, Cousin I, Tabbagh A, Bruand A, Richard G. 2005. Electrical resistivity survey in soil science: A review. *Soil and Tillage Research* **83**(2): 173–193.

Sass O. 2004. Rock moisture fluctuations during freeze-thaw cycles: Preliminary results from electrical resistivity measurements. *Polar Geography* **28**(1): 13–31.

Shaller PJ. 1991. Analysis of a large moist landslide, Lost River range, Idaho, USA. *Canadian Geotechnical Journal* **28**(4): 584–600.

Siebert L. 2002. Landslides resulting from structural failure of volcanoes. In *Catastrophic Landslides: Effects, Occurrence, and Mechanisms*, Vol. **15**. Geological Society of America: Boulder, CO; 209–235.

Socco LV, Jongmans D, Boiero D, Stocco S, Maraschini M, Tokeshi K, Hantz D. 2010. Geophysical investigation of the Sandalp rock avalanche deposits. *Journal of Applied Geophysics* **70**(4): 277–291.

Supper R, Ottowitz D, Jochum B, Römer A, Pfeiler S, Kauer S, Keuschnig M, Ita A. 2014. Geoelectrical monitoring of frozen ground and permafrost in alpine areas: Field studies and considerations towards an improved measuring technology. *Near Surface Geophysics* **12**(1): 93–115.

Tollmann A. 1976. *Analyse des klassischen nordalpinen Mesozoikums; Stratigraphie, Fauna und Fazies der Nördlichen Kalkalpen*. Franz Deuticke Verlag: Wien.

Vidal H. 1953. Neue Ergebnisse zur Stratigraphie und Tektonik des nordwestlichen Wettersteingebirges und seines nördlichen Vorlands. *Geologica Bavarica* **17**: 56–88.

Walter F, Amann F, Kos A, Kenner R, Phillips M, de Preux A, Huss M, Tognacca C, Clinton J, Diehl T, Bonanomi Y, Diehl T. 2020. Direct observations of a three million cubic meter rock-slope collapse with almost immediate initiation of ensuing debris flows. *Geomorphology* **351**(106933): 1–11.

Xu Y, Matsuoka H, Sun D. 2001. Fractal model for grain-size distribution of soils. *Powder and Grains 2001*, 3–6.

Yarnold JC. 1993. Rock-avalanche characteristics in dry climates and the effect of flow into lakes: Insights from mid-Tertiary sedimentary breccias near Artillery Peak, Arizona. *Geological Society of America Bulletin* **105**(3): 345–360.

Supporting Information

Additional supporting information may be found online in the Supporting Information section at the end of the article.

Figure S1: MinMax-Plots of the ERT profiles P1–P4 (a–d) depicting each the modelled inversion with the minimum values (top) and maximum values (bottom) within the error range. Colour differences occur only sparsely and according to the error range at the specific location.

Figure S2: MinMax-Plots of the ERT profiles P5–P8 (a–d) depicting each the modelled inversion with the minimum values (top) and maximum values (bottom) within the error range. Colour differences occur only sparsely and according to the error range at the specific location.

Figure S3: Raw pictures of the gravel pit at Zirmerskopf. (a) and (b) are east–west (E–W)-oriented (rock avalanche flow towards the observer) and were taken on 6 July 2015, (c) was taken on 18 June 2015 looking along the sediment surface to the east.

Figure S4: Grain-size distributions of the two samples from the shear band between two rock-avalanche lobes with fractal dimensions.

Table S1: Parameters of the ERT profiles.

Table S2: Calibration of the ERT profiles with literature data, laboratory tests and field sites.

